Inherited Cardiomyopathies

Spaendonck-Zwarts, Karin Yvon van

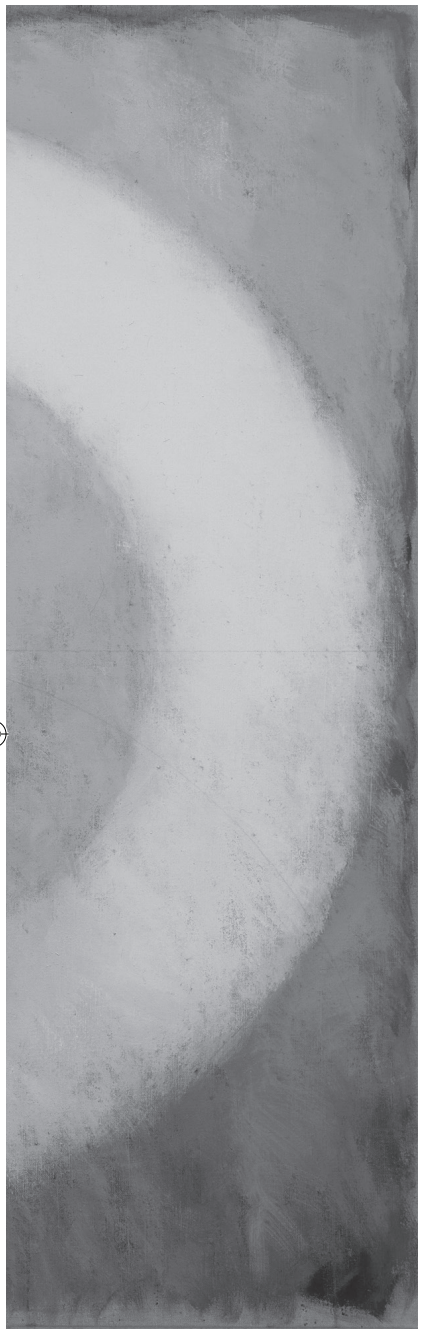

5

Recessive *MYL2* mutations cause infantile type I muscle fibre disease and cardiomyopathy

Marian A.J.Weterman
Peter G. Barth
Karin Y. van Spaendonck-Zwarts
Eleonora Aronica
Bwee-Tien Poll-The
Oebele F. Brouwer
J. Peter van Tintelen
Zohal Qahar
Edward J. Bradley
Marit de Wissel
Leonardo Salviati
Corrado Angelini
Lambertus van den Heuvel
Yolande E.M. Thomasse
Ad P. Backx
Gudrun Nürnberg
Peter Nürnberg
Frank Baas

Brain 2013; 136: 282–293

ABSTRACT

A cardioskeletal myopathy with onset and death in infancy, morphologic features of muscle type I hypotrophy with myofibrillar disorganization and dilated cardiomyopathy was previously reported in three Dutch families. Here we report the genetic cause of this disorder. Multipoint parametric linkage analysis of six Dutch patients identified a homozygous region of 2.1 Mb on chromosome 12, which was shared between all Dutch patients, with a log of odds score of 10.82. Sequence analysis of the entire linkage region resulted in the identification of a homozygous mutation in the last acceptor splice site of the myosin regulatory light chain 2 gene (*MYL2*) as the genetic cause. *MYL2* encodes a myosin regulatory light chain (MLC-2V). The myosin regulatory light chains bind, together with the essential light chains, to the flexible neck region of the myosin heavy chain in the hexameric myosin complex and have a structural and regulatory role in muscle contraction. The *MYL2* mutation results in use of a cryptic splice site upstream of the last exon causing a frameshift and replacement of the last 32 codons by 20 different codons. Whole exome sequencing of an Italian patient with similar clinical features showed compound heterozygosity for two other mutations affecting the same exon of *MYL2,* also resulting in mutant proteins with altered C-terminal tails. As a consequence of these mutations, the second EF-hand domain is disrupted. EF-hands, assumed to function as calcium sensors, can undergo a conformational change upon binding of calcium that is critical for interactions with downstream targets. Immunohistochemical staining of skeletal muscle tissue of the Dutch patients showed a diffuse and weak expression of the mutant protein without clear fibre specificity, while normal protein was absent. Heterozygous missense mutations in *MYL2* are known to cause dominant hypertrophic cardiomyopathy; however, none of the parents showed signs of cardiomyopathy. In conclusion, the mutations in the last exon of *MYL2* are responsible for a novel autosomal recessive lethal myosinopathy due to defects changing the C-terminal tail of the ventricular form of the myosin regulatory light chain. We propose "light chain myopathy" as name for this *MYL2*-associated myopathy.

INTRODUCTION

Infantile fibre-type disproportion with type I fibre hypotrophy, cardiomyopathy and myofibrillar lysis in type I muscle fibres was previously reported in three Dutch families (Barth *et al.*, 1998) and described as a progressive myopathy with onset shortly after birth and a cardiomyopathy leading to death in all patients between four and six months of age. Muscle biopsies showed fibre-type disproportion with small type I and normal sized type II fibres. Ultrastructural analysis showed disorganization of sarcomeres, especially in the smallest fibres, without evidence of storage material (Barth *et al.*, 1998). In all patients, a generalized tremor/clonus was present from birth, even before the cardiomuscular symptoms became predominant. Patients ultimately died of heart failure and shock following progressive cardiac dilatation. Although signs of cardiac strain were present early in the course of the disease, decompensation only occurred in the terminal phase. Autopsies revealed no clues for central nervous system involvement, and a sural nerve biopsy of one patient was normal. Additional features in the first five patients were intermittent mild lactic acidosis not explained by cardiac failure and glycogen depletion in skeletal muscle in the terminal stage of the disease. Two of five patients from the first three described families showed highly increased plasma creatine kinase activities. Despite an extensive search, mitochondrial and fatty acid oxidation defects were not found (Barth *et al.*, 1998). Because both sexes were affected, all parents were apparently healthy, and some families had more than one affected child, the disease was thought to result from autosomal recessive mutations. We therefore set out to identify the gene involved in this disorder and succeeded in identifying three different mutations, all affecting the same exon of the same gene, myosin regulatory light chain 2 (*MYL2*), as the underlying genetic cause of this disorder. Dominant mutations in *MYL2* were already known to cause hereditary ventricular hypertrophy or hypertrophic cardiomyopathy (HCM) (Poetter *et al.*, 1996; Flavigny *et al.*, 1998; Andersen *et al.*, 2001; Richard *et al.*, 2003; Kabaeva *et al.*, 2002). Also, defects in the *MYL3* and *MYH7* genes that encode the other components of the β-cardiac myosin, the cardiac essential light chain and myosin heavy chain, respectively (CMH8; OMIM #608751; CMH1; OMIM #192600) are known to cause HCM. Here we report three different recessive mutations in *MYL2*, which are the cause of myopathy, fibre type I hypotrophy with myofibrillar disarray and cardiomyopathy.

MATERIALS AND METHODS

Patients

All patients were referred to university centres for diagnosis and treatment. Genomic DNA was isolated from blood samples of patients and relatives according to standard diagnostic procedures. DNA analysis and further cardiologic examinations were carried out after a genetic counseling procedure and consent of the relatives. Muscle biopsies were obtained for diagnostic reasons. Stored specimen from these biopsies, as well as frozen and paraffin embedded tissue of the deceased patients, were made available by the Departments of Pathology of the University

Medical Centre Leiden, University Medical Centre Groningen and the Academic Medical Centre Amsterdam.

Enzyme and immunohistochemistry

Immunohistochemical stainings were performed according to standard staining procedures. For the MYL2 stainings, paraffin sections of muscle tissue of deceased patients as well as control muscle tissue were deparaffinized in xylol, followed by rehydration in a series of ethanol solutions, after which antigen retrieval was carried out by boiling in 10 mM citrate buffer supplemented with 0.05% Tween-20 for 2 minutes in a microwave. After preincubation in a buffer containing 2% goat serum, 0.1% bovine serum albumin and 0.5% Triton™ X-100, incubation with the primary antibody was performed overnight at 4ºC (Epitomics 17-1 and 42-2; 1:100) followed by blocking endogenous peroxidase (0.3% H_2O_2 in PBS supplemented with 0.1% Tween-20) before incubation with a peroxidase-coupled goat-anti rabbit secondary antibody (Brightvision, Immunologic) and detection using the NovaRED™ system (Vector Laboratories). Frozen tissue sections were fixed using methanol or acetone before primary antibody incubation, omitting the antigen retrieval step. Slides were counterstained using hematoxylin before rehydration and mounted onto slides using Vectamount™ (Vector Laboratories). Images were captured using an Olympus BX41 microscope, equipped with a DP25FW camera and CellD software. Slow (Hybridoma Bank; clone A 4.951; 1:100) and fast (Biogenex / MU109-UC, clone MY-32; 1:200) myosin staining was performed on paraffin sections according to routine diagnostic procedures. Frozen 6 µm-thick sections prepared from muscle biopsies were routinely stained for hematoxylin and eosin and Gomori trichrome, ATPase preincubated at pH 4.3, nicotinamide adenine dinucleotide tetrazolium reductase (NADH), succinate dehydrogenase, periodic acid Schiff, periodic acid Schiff-diastase and Oil red O. Frozen tissue sections stained for ATPase activity after preincubation at pH 4.3 were used for muscle morphometry as described (Dubowitz, 1985).

Protein isolation and western blot analysis

Proteins were extracted from minced tissues using ice-cold lysis buffer containing 50 mM Tris/HCl, pH 7.4, 150 mM sodium chloride, 1 mM EDTA, 1% Triton™ X-100 and 0.1% sodium dodecyl sulfate, supplemented with protease inhibitor cocktail (Roche). After incubation of 2 minutes in a bath sonicator followed by incubation for 5 minutes at 95ºC, the samples were mechanically homogenized as much as possible. Protein concentrations were determined using the Pierce BCA Protein Assay kit. Proteins were separated on a 15% sodium dodecyl sulfate polyacryl amide gel electrophoresis (SDS-PAGE) and transferred onto polyvinylidene fluoride membrane (Millipore) by semi-dry electroblotting. Blots were preincubated in PBS supplemented with 2% goat serum, 5% bovine serum albumin, 0.1% Triton™ X-100 and 0.1% dimethylsulphoxide before incubation with the primary antibody for 12-16h at 4 ºC. Dilutions of the primary antibodies used were 1:1000 for antibody 2917-1 (Epitomics), 1:10000 for antibody

2742-1 (Epitomics), and 1:2000 for GAPDH (Millipore MAB374/clone 6C5). Subsequently, the blots were incubated with species-specific horseradish peroxidase-coupled secondary antibodies (Dako, 1:2000), and the resulting signals were visualized using the Lumi-lightPLUS western blotting substrate (Roche) and a LAS-3000 luminescent image analyzer (Fuji Film).

Linkage analysis

DNA samples from six affected infants were genotyped using the Affymetrix GeneChip® Human Mapping 250K Sty Array as described before (Budde *et al.*, 2008). The gender of samples was verified by counting heterozygous single nucleotide polymorphisms (SNPs) on the X chromosome. Relationship errors were evaluated with the help of the program Graphical Representation of Relationships (GRR) (Abecasis *et al.*, 2001). For log of odds (LOD) score calculations, we assumed six consanguineous families with one child from second cousin marriages, an approach useful for identification of rare recessive disorders when consanguinity was not proven *a priori* (Rutsch *et al.*, 2009). Linkage analysis was performed assuming autosomal recessive inheritance, full penetrance and a disease allele frequency of 0.0001. Multipoint LOD scores were calculated using ALLEGRO (Gudbjartsson *et al.*, 2000). Haplotypes were constructed with ALLEGRO and presented graphically with HaploPainter (Thiele and Nurnberg, 2005). All data handling was done using the graphical user interface ALOHOMORA (Ruschendorf and Nurnberg, 2005).

Next generation and Sanger sequencing

Sequence capture was performed using a custom design 385K capture array (chr12: 108,060,000-110,350,000; hg18/NCBI36) according to the protocol supplied by the manufacturer (Roche). Briefly, a representing library was made of patient DNA sheared to an average length of 500-800 bp by cavitation (Covaris). After hybridization, DNA enriched for target sequences was amplified, quantified (Qubit) and analyzed on a Bioanalyzer DNA 7500 chip (Agilent) followed by pyrosequencing on a Roche FLX titanium sequencer. Analysis was performed with the Newbler program (v2.3, Roche). Approximately $1.1x10^6$ filter-passed reads were obtained from $1.8x10^6$ key passed sequences. Twenty-six per cent of mapped reads were uniquely mapped to the target region and were scanned for differences with the human consensus sequence using the Roche software. All high confidence differences as defined by the manufacturer were analyzed for their heterozygous or homozygous state, position in relation to coding exons and surrounding boundaries, known occurrence as polymorphisms, and potential effect on the protein.

Direct Sanger sequencing was performed with primers flanking the exons. Amplification was performed with exon-specific M13-tagged primers using 20 ng of genomic DNA, 4 mM $MgCl_2$, HOT FIREPol™ DNA polymerase (Solys Biodyne) and a touchdown PCR program. Primer sequences used are supplied in Supplementary *table 1*. The resulting PCR products were treated with shrimp alkaline phosphatase and exonuclease I before sequencing using the

ABI Big Dye Terminator cycle sequencing kit V1.1 and an ABI3730xl sequencer (Applied Biosystems). Exome sequencing was performed using the SOLiD™ 4 System according to the manufacturer's protocol with the exception of small fragment removal, which was performed using Agencourt® AMPure® Beads XP; $4.2x10^8$ of total reads yielded $1.6x10^8$ aligned reads of which 62% could be aligned in pairs. Analysis was performed using the Varscan and Bioscope software programs. For graphic representation, the Integrated Genome Viewer (IGV) was used.

Reverse transcriptase polymerase chain reaction

Total RNA was isolated from frozen diaphragm tissue of N-C2 using TRIzol® according to the manufacturer's protocol (Invitrogen). A first strand reaction performed on 5 μg of total RNA primed by oligo-dT-VN was used for a reverse transcriptase reaction using Superscript® II (Invitrogen) followed by heat inactivation and RNase H treatment before amplification using a touchdown PCR program and intron-spanning primers (see Supplementary data, *Table S1* for sequences).

Cardiologic examination

Parents who consented to evaluation were interviewed for signs of neuromuscular weakness or cardiac complaints, including rhythm disturbances, and underwent cardiologic evaluation by 12-lead ECG and echocardiography. Specific attention was given to signs indicative of any type of inherited cardiomyopathy (i.e. hypertrophic, dilated, restrictive or non-compaction cardiomyopathy).

RESULTS

Clinical characteristics of patients

We identified 11 affected infants from eight different Dutch families and two affected infants from one Italian family with similar clinical and biopsy findings (*Table 1*). All patients were born at term after uncomplicated pregnancies, with normal birth weight and length, and no outward signs of malformation. The only sign of distress at birth was a coarse clonus/tremor. This generalized high amplitude tremor or clonus was present in all patients before the onset of cardiac or neuromuscular symptoms. It was present while awake, absent during sleep and strikingly resembled the hyperexcitation syndrome, known in distressed newborns. However, none of the affected babies had perinatal problems. Hypoglycaemia and hypocalcaemia were excluded. The tremor slowly abated over a period of weeks. No other symptoms pertaining to the central nervous system were present. No cerebral abnormalities were found in routine autopsies, except one case with hypoxic-ischaemic damage due to postnatal circulatory failure. Patients were vigorous at birth without signs of muscle weakness, or other signs of prenatal muscle involvement such as contractures or polyhydramnios. All patients had rapidly progressive generalized muscle weakness starting within weeks after birth and the majority had a tented mouth or global facial muscle involvement (*Figure 1A and B*). All patients died of

heart failure due to cardiomyopathy, which was mainly dilated although some patients had features of other forms of cardiomyopathy (hypertrophic, restrictive or non-compaction)(*Table 1*). All had similar muscle biopsies morphologically characterized by fibre-type disproportion with type I fibres and normal-sized type II fibres. Fibre size disparities ranged between 48 and 79% (n<12%) (*Table 1, Figure 1C and D*). Electron microscopy of muscle biopsies showed abnormalities varying between loss of register between adjacent sarcomeres in normal or small sized fibres to severe disorganization and loss of myofibrils in the smallest fibres without storage material (*Figure 1E*). No loss of mitochondria was seen in affected fibres with myofibrillar disorganization (*Figure 1D and E*). Plasma creatine kinase levels were increased and very high in several patients. This finding mirrors the rapid clinical progression and the observed histopathological changes, such as subendocardial fibrosis and myofibrillar disorganization in skeletal muscle (*Table 1*).

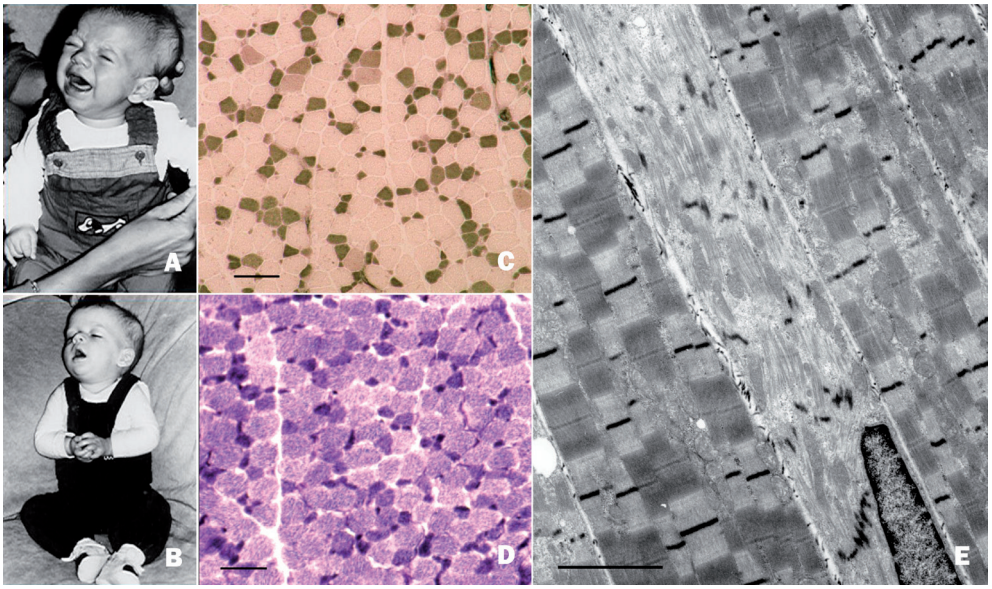

Figure 1: Summary of clinical histories and biopsy findings.
(*A*) Patient N-A1 at 1-2 months: crying with normal facial expression, (*B*) at 5 months: general limpness with facial palsy and ptosis. Reproduced with written consent of the parents. (*C*) Light microscopy of quadriceps muscle (of patient N-B10), frozen section, staining for myosin ATPase activity (pH 4.3) showing fibre-type disproportion with increased diameter variability and smallness of type I fibres. Scale bar = 50 µm. (*D*) Quadriceps muscle, frozen section, NADH oxidoreductase reaction showing fibre-type disproportion of the same sample. Smallest (dark) type I fibres show increased activity. Scale bar = 50 µm. (*E*) Electron microscopy of quadriceps muscle of patient N-D1. Central fibre shows severe disarray of normal sarcomeric structure including Z-disks and lysis of myofibrils. Adjacent fibres show loss of register of sarcomeres. Scale bar = 1 µm.

Table 1: Clinical characteristics of patients

Patient; number of affected siblings [a]	Sex	Month [b]	Tremor/ clonus	Progressive myopathy; creatine kinase (U/l)	Cardiomyopathy	Autopsy	Fibre-type disproportion	Additional data: electron microscopy of small fibres; respiratory chain in skeletal muscle
N-A1[a]; 2/2	M	6	Yes	Generalized, tented mouth, ptosis; 50 U/l	Acute decompensation following infection shortly before death	General cardiac dilatation with slight hypertrophy	Quadriceps m. I: 6.0 ± 3.3 µm, II: 17.8 ± 3.6 µm; FSD 66; 70% type I; paucity type 2B fibres	EM: severely disorganized sarcomeres, partial loss of myofibrils, no loss of mitochondria; RC: no abnormalities
N-A2[a]; 2/2	F	6	Yes	Generalized, tented mouth; 26 U/l	Dilated, decompensation	General cardiac dilatation with slight hypertrophy	Quadriceps m. I: 4.9 ± 3.3 µm, II: 13.0 ± 1.6 µm; FSD 62; 69 % type I; paucity type 2B fibres	EM: severely disorganized sarcomeres, partial loss of myofibrils, no loss of mitochondria; RC: no abnormalities
N-B10[a]; 2/10	F	5	Yes	Generalized, tented mouth; 134 U/l	Dilated, decompensation	ND	Quadriceps m. I: 10.2 ± 4.3 µm, II: 17.1 ± 6.4 µm; FSD 48; 48% type I; paucity type 2B fibres	EM: severely disorganized sarcomeres, partial loss of myofibrils, no loss of mitochondria; RC: no abnormalities
N-C2[a]; 2/2	F	5	Yes	Generalized, terminal rhabdomyolysis; 1733 U/l	Dysfunction both ventricles, FS 11%, cardiogenic shock and multiorgan failure	Cardiac dilatation, hypoxic–ischaemic brain damage	Quadriceps m. I: 7.6 ± 3.5 µm, II: 14.0 ± 2.8 µm; FSD 79; 79% type I; paucity type 2B fibres	EM: severely disorganized sarcomeres, partial loss of myofibrils, no loss of mitochondria; RC: no abnormalities
N-D1; 1/1	F	4	Yes	Generalized, tented mouth; 712 U/l	Restrictive, cardiogenic shock	Cardiac hypertrophy and dilatation, interstitial fibrosis, subendocardial fibrosis LA	Quadriceps m. I: 6.7 ± 2.5 µm type 2A: 15.2 ± 2.5 µm; FSD 56; 70% type I	EM: severely disorganized sarcomeres, partial loss of myofibrils, no loss of mitochondria; RC: decreased oxidation of radiolabelled substrates and pyruvate oxidation
N-E1; 3/4	M	5	Yes	Generalized; ND	Acute decompensation	Dilated cardiomyopathy, fibroelastosis LA and RV	Present, no quantitative data	
N-E2; 3/4	M	5	Yes	Generalized; 9 U/l	Decompensation	ND	Anterior tibial m. I: 8.6 ± 7.9 µm, 2A: 21.65 ± 4.9 µm; FSD 60; 62% type I	EM: severely disorganized sarcomeres, no loss of mitochondria

N-F1; 1/1	M	5	Yes	Generalized, tented mouth; 46 U/l	Dilated, restrictive and slightly hypertrophic LV, decreased contractility	Dilated cardio-myopathy, subendo-cardial, interstitial and perivascular fibrosis	Quadriceps m. I :6.2 ± 1.3 µm, 2A 15.5 ± 2.2 µm; FSD58; 59% type I	EM: disorganized sarcomeres; RC: decreased oxidation of radiolabelled substrates and pyruvate oxidation, slight reduction activity complex II
N-G1; 1/1	F	1	Yes	Generalized from birth; 32–204 U/l (*n* = 7)	Non-compaction	Cardiac non-com-paction	Quadriceps m. I: 6.4 ± 2.8 µm, 2A: 12.5 ± 3.5 µm; FSD 49; 45% type I	RC: no abnormalities
N-H1; 2/2	F	6	Un-known	Generalized, proximal > distal, diaphragmatic respiration, tented mouth; 106–5116 U/l (*n* = 8)	Dilated	Cardiac dilatation, thinning RV	Quadriceps m. I: 6 ± 1.0 µm, 2A: 12.8 µm ± 1.9 µm; FSD 53; 57 % type I	
N-H2; 2/2	M	5	Yes	Generalized, tented mouth; 41–425 U/l (*n* = 6)	RV and septal hypertrophy, insuf-ficiency mitral valve, restrictive cardio-myopathy	ND	Quadriceps m. I: 7.2 µm ± 3.0 µm, 2A: 14.5 ± 3.0 µm; FSD 50; 67% type I	EM: severely disorganized sarcomeres
I-A2; 2/3	M	6	Yes	Generalized weakness, facial muscles affected; 450 U/l	Dilated, slightly hypertrophic	ND	Quadriceps m. I: 4.5 ± 1.9 µm, 2A: 11.2 ± 2.4 µm, 2B: 11.5 ± 2.7; FSD 53; 51% type I	EM: myofibrillar disarray; RC: no abnormalities
I-A3; 2/3	M	6	Yes	Generalized weakness, facial muscles affected; 412 U/l	Normal at birth, markedly dilated at 5 months, slightly hypertrophic LV with decreased contractility, FS 18%, evidence of LV non-compaction.	ND	Present, no quantita-tive data	

Siblings born with the help of in vitro fertilization with sperm or egg cell donation of other persons than the parents of the named patients were excluded from the total number of siblings. [a] Patients previously published by Barth *et al*., 1998. [b] Died in months (mo) after birth.
CK = creatine kinase; EM = electron microscopy; FS = fractional shortening; LA = left atrium; LV = left ventricle; ND = not done; RA = right atrium; RC = respiratory chain; RV = right ventricle. FSD = fibre size disparity = µ2 − µ1/µ2 × 100 where µ2 and µ1 represent mean diameters of type II and type I fibres.

Identification of the genetic cause

Based on the rare occurrence of this disorder, we assumed a recessive monogenic cause for the disease in the Dutch families, and performed a genome-wide search for regions of homozygosity shared between six Dutch patients (N-A1, N-B10, N-C2, N-D1, N-E1, N-F1) from six different families, using a 250 K Affymetrix® StyI SNP microarray. We assumed consanguinity as well as full penetrance, an autosomal recessive mode of inheritance and a disease allele frequency of 0.001. By multipoint parametric linkage analysis using a reduced panel of SNPs (approximately 20.000), we identified a single peak on chromosome 12 with a maximum LOD score of 9.8. Analysis of the critical region with all markers gave a maximum LOD score of 10.8, indicating that this region must harbor the disease-causing mutation. An identical haplotype for this region could be constructed for all Dutch patients defined by the limiting SNPs rs10849988 and rs10849946 located at a distance of 2.1 Mb (*Figure 2*).

We set out to identify the pathogenic mutation by sequencing of the 2.1 Mb region. We designed a custom 2.3 Mb Nimblegen array for sequence capture that covered the entire linkage region (chr12:108,060,000-110,350,000 NCBI36/hg18) and used genomic DNA from N-D1 to enrich for these target sequences. Analysis on an FLX Titanium 454 sequencer (Roche) yielded 1.1 million filter-passed sequences with a median length of 370 bp, which were mapped to the human consensus genome (hg18) with Newbler software. Twenty-six per cent of the reads mapped to the captured region, which contained 31 annotated genes, one hypothetical locus, one mitochondrial RNA locus and three pseudogenes. More than 95 % of all exons were sequenced with coverage of more than eight times. Analysis yielded 1192 reliable nucleotide changes. Because the mode of inheritance is autosomal recessive, the expected disease-causing mutation would be a homozygous change. Within the coding regions of annotated genes and

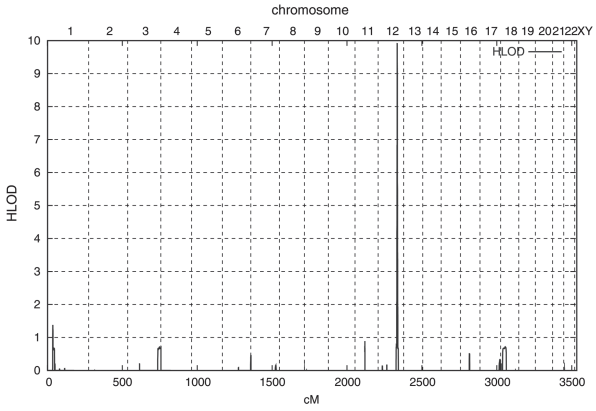

Figure 2: Linkage analysis of six Dutch patients identifies the region containing the causative gene. The heterogeneity LOD (HLOD) score, presented on the y-axis, is plotted against the genetic position in cM on the X-axis starting from the tip of chromosome 1 through the the q-arm of chromosome 22, followed by sex chromosomes X and Y.

adjacent intronic sequences (within 20 nucleotides of the exon-intron boundaries), we found 49 homozygous nucleotide variations, most of which were located in the non-coding 3'tails of the last exons. Fifteen variations were located in the coding regions, and eight of these were predicted to lead to an amino acid change, however, these were all annotated as known polymorphisms (www.ncbi.nih.gov).

A homozygous splice site mutation (c.403-1G>C) was detected in the last acceptor splice site of the *MYL2* gene when the threshold was reduced to six-times coverage. Sanger sequencing was used to obtain sufficient coverage of all coding regions that did not reach the level of eight-times coverage. This analysis confirmed the presence of the found splice site mutation as the only mutation not annotated as a polymorphism in the entire linkage interval. Additional sequence analysis of the other five Dutch patients showed the same homozygous mutation in all patients. Three additional Dutch patients (N-G1, N-H1, N-H2) with similar clinical characteristics that were not included in the linkage analysis also carried the same homozygous mutation. Of seven families, DNA from the parents was available and upon testing, they were all shown to be heterozygous carriers.

Owing to the location of the mutation, just before the last exon, the mutant messenger RNA is not expected to be prone to nonsense-mediated decay, and whole exon skipping also cannot occur within the normal transcript. Because the mutation most probably will affect splicing, we screened the genomic sequences of intron 6 for the presence of cryptic splice sites using splice prediction program NNSplice and, consequently, designed several reverse transcriptase PCRs (based on the use of these sites). Analysis of the messenger RNA from muscle tissue (diaphragm) of patient N-C2 using a forward primer spanning the exon 5-6 junction and one of a number of reverse primers downstream of the predicted sites, showed that a cryptic splice site 23 nucleotides upstream of the original splice site is used (*Figure 3, Figure S1*). This results in a frameshift mutation and replacement of the last 32 codons by 20 different codons and thus alters the C-terminal part of the protein.

Figure 3: RNA expression analysis shows presence of mutant *MYL2* messenger RNA.
Reverse transcriptase PCR on muscle tissue of patient N-C2. Lane M contains the 1 kb ladder (Invitrogen), Lanes R1 and R2 contain the exon-spanning reverse transcriptase PCR products obtained with reverse primers R1 and R2. The forward primer (F) overlaps the transition of exon 5 and exon 6. Wt = wild type.

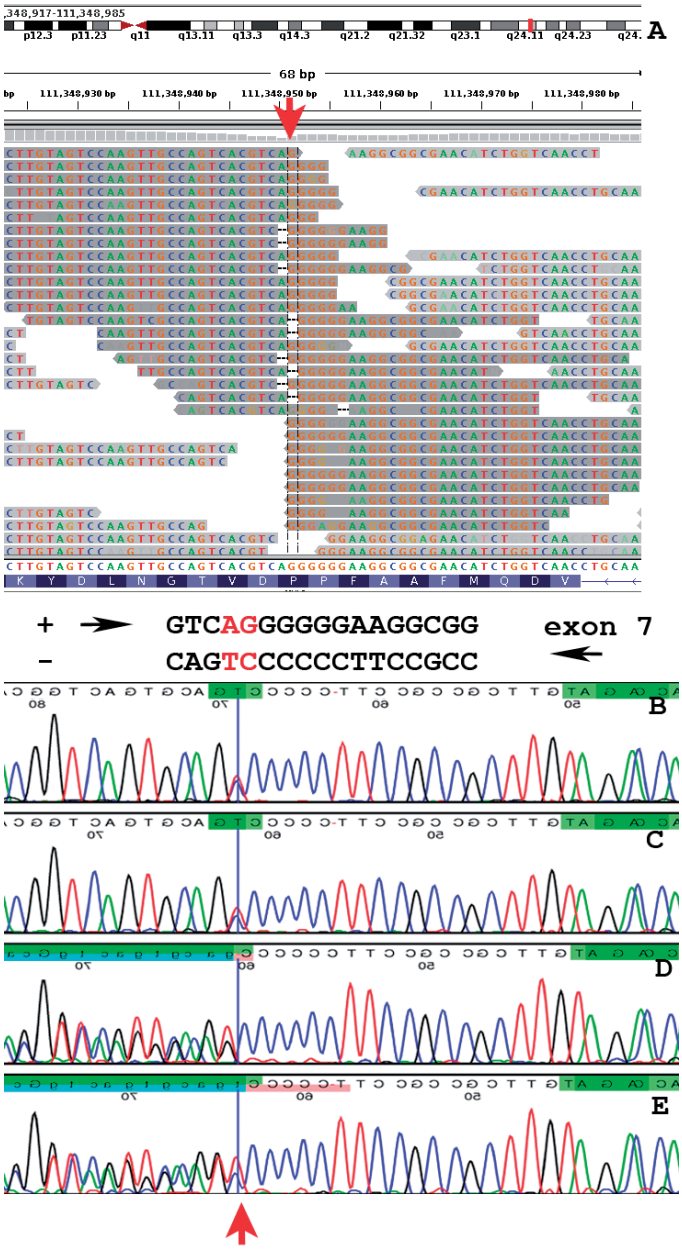

Figure 4: Sanger and exome sequence analysis demonstrates the presence of two different *MYL2* mutations in the Italian family.
(*A*) The plus strand of the genome around the *MYL2* mutation (red arrow|) is shown as presented using Integrated Genome Viewer. (*B-E*) Sanger sequence analysis shows the coding *MYL2* strand (minus strand of genome) for I-A2 (*B*), I-A3 (*C*), and their parents (*D,E*).

Whole exome sequencing of the Italian patient (patient I-A2) demonstrated compound heterozygosity for two other mutations, c.431delC; p.Pro144LeufsX2 and c.432delT; p.Asp145ThrfsX2, affecting two adjacent nucleotides in the last exon of the *MYL2* gene. Sanger sequencing of the parents indeed demonstrated that the patient had inherited one defective allele with a deletion of one nucleotide from each parent (*Figure 4*). Both changes result in a frame shift and premature termination in the third codon of the shifted open reading frame (original codon 146), leading to mutant truncated proteins that are 20 amino acids shorter than the normal protein.

Expression of the protein

The use of two commercially available antibodies (Epitomics), one that recognizes an epitope in the C-terminal tail (antibody 2742-1) and another more centrally located (antibody 2917-1), enabled us to discriminate between normal and mutant protein. In control muscle tissue, normal protein was detected at a high level in the muscle fibres that were identified as type I fibres by additional staining against slow and fast myosin. In patients, the level of expression was lower, ranging from moderate to hardly detectable with antibody 2917-1, which should detect both normal and mutant protein. Moreover, fibre type specificity had disappeared (*Figure 5*). The second, C-terminal MYL2 antibody (2742-1) showed the same fibre type I-specific pattern in normal muscle tissue, while normal MYL2 was absent in all seven patients examined (*Figure 5 and Figure S2*), which is in line with the predicted loss of the epitope detected by antibody 2742-1. The loss of the C-terminal epitope was confirmed by western blot analysis of post-mortem muscle tissue of patients N-C2 and N-F1 (*Figure 6*). Biopsy muscle tissue from patients N-H1 and N-H2 gave the same result (not shown). Owing to poor performance of an-

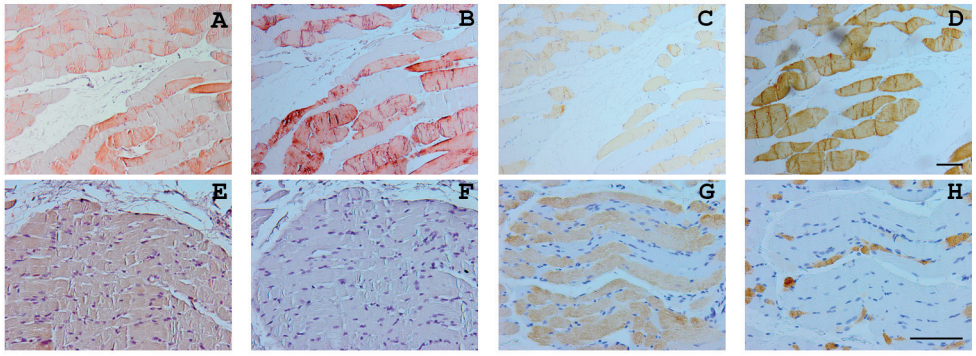

Figure 5: MYL2 expression in control and patient muscle sections.
Immunohistochemical staining using MYL2 antibodies 2917-1 (*A,E*) and 2742-2 (*B,F*), anti-fast myosin (*C,G*) and anti-slow myosin (*D,H*) antibodies on paraffin embedded serially cut sections of control muscle tissue (*A-D*) and muscle tissue from patient N-C2 (*E-H*). For identification of fibre type, the specific staining for fast/slow myosin was used. Additional staining results on frozen sections are supplied in *Figure S1*. *A-D*: x10 magnification; *E-H*: x20 magnification. Scale bars: *D* and *H* = 100 µm.

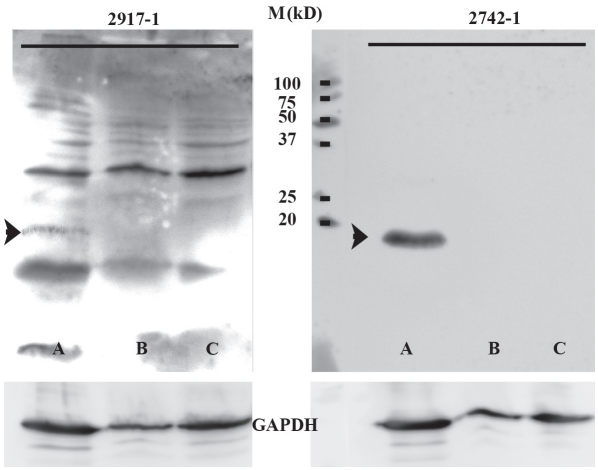

Figure 6: Western blot analysis of MYL2 expression in control and patient muscle shows loss of C-terminal epitope in patients.
Western blot analysis of post-mortem muscle tissue of a control (*A*), patients N-C2 (*B*) and N-D1 (*C*) using the C-terminal antibody 2742-1 (right) or antibody 2917-1 (left). The arrow indicates the size of the MYL2 protein. As a loading control, expression of GAPDH is shown (bottom). As a size marker, the Precision-Plus Protein™ Dual Coleur standards were used (Bio-Rad).

tibody 2917-1, which was raised against an epitope present in both mutant and normal MYL2, a band of the same size was only seen as a faint signal in control tissue, whereas it was below detection level in the patients despite loading of comparable amounts of protein.

Cardiologic evaluation of heterozygous carriers

Because dominant missense mutations in *MYL2* have been reported in adults with hypertrophic cardiomyopathy (HCM), all available parents (n=14) were subjected to cardiologic evaluation. No indications for cardiomyopathy were found. Only a structural variation consisting of an accessory papillary muscle in the left ventricular apex and on the septum was seen in one of the parents, which is not indicative of a cardiomyopathy.

DISCUSSION

We identified three different mutations in *MYL2* as the causative gene defects causing the present disease, thereby enabling prenatal molecular screening for this fatal disorder.
Heterozygous dominant *MYL2* mutations were previously described in patients with HCM, but no reports have linked mutations in this gene with skeletal myopathies. All Dutch patients shared the homozygous c.403-1G>C mutation, indicative of a founder mutation, whereas in an Italian family two compound heterozygous mutations were found. All three mutations target the last exon of the gene.

MYL2, also known as *MLC-2V* encodes the cardiac, ventricular isoform of myosin regulatory light chain, which is part of the slow-twitch skeletal muscle myosin complex as well as the β-cardiac complex. Myosins, encoded by a multigene family, are large hexameric motor proteins that bind actin and convert energy from ATP hydrolysis into mechanical force. They consist of two heavy chains, two essential light chains and two regulatory light chains. The heavy chains consist of a long rod-like tail, the flexible neck-region and the head region where binding to actin as well as hydrolysis of ATP occurs. Heavy chain isoform profiles determine the specific physiological properties of the muscle fibres (Weiss and Leinwand, 1996). In mammalian skeletal muscles, four major fibre phenotypes are distinguished: slow-twitch or type I fibres (*MYH7*) and three types of fast-twitch types (*MYH2, MYH1, MYH4*): type IIa, IIb, and IIx/d fibres (summarized in Schiaffino and Reggiani, 2011; see *Table 2*). In humans, three fibre types exist: slow/type I fibres (*MYH7*) and two types of fast fibres, type 2A (myosin IIa/*MYH2*) and type 2B (myosin IIx/*MYH1*). Although *MYH4* is present in the human genome and MYH4 is the predominant heavy chain in mouse type IIb fibres, the human protein is absent despite expression at the RNA level in foetal muscle and certain conditions such as Duchenne muscular dystrophy (Harrison *et al.*, 2011). Both (essential/alkali and regulatory) light chains bind to the neck region that functions as a lever arm in the myosin complex and have a structural role in actomyosin sliding velocity (Lowey *et al.*, 1993; Uyeda and Spudich, 1993). Essential light chains

Table 2: Global scheme of main myosins and major muscle fibre types in adult human skeletal muscle and heart

Myosin	Adult heart	Myosin Gene	Adult skeletal muscle	Myosin Gene
Myosin heavy chain	Type α, atrial isoform	*MYH6*	Type 2A: myosin IIa, fast Ype 2B: myosin IIx/d, fast	*MYH2* *MYH1*
	Type β, ventricular isoform	*MYH7*	Type 1, slow	*MYH7*
Myosin essential/ alkali light chain	Atrial isoform	*MYL1(MYL4)*	Fast	*MYL1*
	Ventricular isoform	*MYL3*	Slow	*MYL3 (MYL6B)*
Myosin regulatory light chain	Atrial isoform	*MYL7*	Fast	*MYLPF*
	Ventricular isoform	*MYL2*	Slow	*MYL2*

Myosins expressed in highly specialized tissue and embryonal en perinatal isoforms are not included in this table except for the embryonic/atrial isoform *MYL4/MLC1A* (between brackets) which is also expressed in the atrium. *MYL6B* (between brackets), also known as *MLC1sa*, is also expressed in non-muscle cells. *MYL-PF* is also known as *MLC2B* or *HUMMLC2B*. *MYL1* encodes two isoforms, *MLC1F* and *MLC3F*. Regarding the composition/expression; in addition to "pure" fibres, many hybrid fibres exist owing to anatomical location and interindividual variability.

have been shown to be essential for full force production (VanBuren *et al.*, 1994) by altering actomyosin cross-bridge kinetics, as has been demonstrated in transgenic mice carrying a human pathogenic mutation that causes hypertrophic cardiomyopathy (HCM) (Muthu *et al.*, 2010). In contrast to the essential light chains, the regulatory light chains can be phosphorylated leading to a conformational change, which consequently affects muscle contraction. More isoforms of (regulatory) light chain genes also exist that encode different light chain isoforms possibly fulfilling different physiological requirements (*Table 2*). The light chains that predominate in slow twitch-muscle are the same as those in the cardiac ventricle. In contrast, the atrial form of myosin regulatory light chain (*MYL7/ MLC-2a/MYL2A*), is not expressed during skeletal myogenesis or in skeletal muscle (Hailstones *et al.*, 1992).

The *MYL2* mutations that we identified all cause frame shifts either directly as a consequence of the mutation or through use of an alternative splice site that will consequently lead to mutant proteins with altered C-terminal tails. Normal MYL2 was undetectable in tissue sections of skeletal muscle of seven Dutch patients from six families, whereas mutant protein expression was weak, diffuse and without the expected type I-specific expression. Subsequent western blot analysis indeed showed absence of wild-type MYL2 in the patients when using the C-terminal antibody. Although mutant messenger RNA was clearly present in muscle post-mortem tissue from patient N-C2, this apparently did not lead to a protein expression level comparable to that in control tissue, which suggests that the pathogenic mechanism is one of (partial) loss of function which would be expected for a recessive mutation. Loss of fibre type-specific expression may result in a compensation mechanism as has been described for the heavy chain of myosin as a result of physical stress or disease. In heart muscle in rodents, a shift takes place from the predominant α-type (Myh6) towards the foetally expressed β-type isoform (Myh7) through a microRNA-dependent mechanism (van Rooij *et al.*, 2007). In contrast, human adult healthy hearts are mostly composed of the β-type (MYH7) in addition to a small fraction of α-fibres (MYH6). In failing human hearts, a shift toward more myosin heavy chain β-fibres is also observed due to downregulation of the α-isoform (Nakao *et al.*, 1997; Hang *et al.*, 2010). Downregulation of MYL2 was found to be associated with chronic heart failure (Li *et al.*, 2011). In heart tissue sections of two of our patients, staining was hardly seen if not absent at all (*Figure S3*), whereas normal expression was clearly visible in the control sections. Because we could demonstrate the presence of the mutant *MYL2* messenger RNA, we expected to see some expression of the mutant MYL2 protein in muscle. The diffuse staining seen in the skeletal muscle paraffin sections without fibre-type specificity that was lacking in control muscle sections must be due to residual expression of mutant MYL2 regardless of the fibre type or to upregulation of a cross-reacting protein, which may be a highly homologous myosin light chain member. In comparison to control tissue, the staining is strongly reduced in patient tissue.

Selective type I hypotrophy occurs as part of many congenital myopathies. In congenital fibre-type disproportion, hypotrophy of type I fibres is the single remaining histologic abnormality without more specific findings (Clarke and North, 2003). Sarcomere gene mutations constitute

a growing part of disorders, previously labeled as congenital fibre-type disproportion. In addition to nemaline myopathies (Sanoudou and Beggs, 2001), hypotrophy of type I fibres can be caused by dominant mutations in tropomyosins *TPM2* and *TPM3* (Brandis *et al.*, 2008; Clarke *et al.*, 2008) or skeletal α-actin (*ACTA*) (Laing *et al.*, 2004) and recessive mutations in the genes coding for ryanodine receptor (*RYR1)* (Clarke *et al.*, 2010), and selenoprotein (*SEPN1*) (Clarke *et al.*, 2006).

Interestingly, mutations in *MYH7*, which encodes the β-cardiac myosin heavy chain (the heavy chain partner of MYL2), are accompanied by fibre-type disproportion in a few cases. Mutations in the rod region are mostly associated with myosin storage myopathy or Laing's myopathy, whereas *MYH7* mutations in the globular region, which contains the binding site for the light chains, mostly cause HCM without skeletal muscle involvement (Kelly and Strauss, 1994; Laing *et al.*, 1995; Tajsharghi *et al.*, 2003; Walsh *et al.*, 2010). Two cases with mutations in the rod region were reported with type I hypotrophy together with or without a myosin storage myopathy in one case each (Muelas *et al.*, 2010; Ortolano *et al.*, 2011). One report described a mutation in the neck region of *MYH7* in a patient with type I hypotrophy as well as a cardiomyopathy (Darin *et al.*, 2007). No previous reports have linked *MYL2* to fibre type I hypotrophy. Our study shows that C-terminal recessive mutations in *MYL2* result in a cardiomyopathy and skeletal myopathy with morphologic features of type I hypotrophy in addition to myofibrillar disorganization, leading to a severe disease phenotype.

MYL2 specifically binds to the myosin heavy chain (Wadgaonkar *et al.*, 1993) and its phosphorylation was reported to be important in regulation of myosin ATPase activity in smooth muscle cells and of non-muscle-myosin (Macera *et al.*, 1992). In striated muscle, an increase in calcium concentration triggers contraction via the troponin/tropomyosin pathway, which controls the actin-myosin interaction. The identification of *MYL2* mutations in adults with HCM demonstrated their relevance in striated muscle as well. A spatial gradient of phosphorylated MYL2 across the heart has been described in human, mouse and rabbit cardiac tissue to facilitate cardiac contraction (Davis *et al.*, 2001). MYL2 belongs to the EF-hand superfamily of proteins, with two EF-hand-motifs capable of calcium-binding. EF-hands are found in pairs or higher copy numbers and form a structure implied to function as a calcium sensor and modulator of calcium signaling. The binding of calcium can cause a conformational change and may affect the structure of both EF-hands (Wimberly *et al.*, 1995), thus affecting interaction with downstream targets (Grey *et al.*, 2005). Ten different *MYL2* mutations have been reported to date as the probable cause for HCM, six of which are dominant missense mutations located in or near the region containing the N-terminal EF-hand or phosphorylation-binding site (Andersen *et al.*, 2001; Flavigny *et al.*, 1998; Kabaeva *et al.*, 1992; Poetter *et al.*, 1996; Richard *et al.*, 2003; Szczesna-Cordary *et al.*, 2004; Szczesna-Cordary *et al.*, 2005; Kerrick *et al.*, 2009) (*Figure 7*). All six dominant pathogenic mutants were functionally tested and all affected myosin function (Szczesna *et al.*, 2001). In a transgenic mouse model where approximately 10% of cells expressed mutant A13T instead of endogenous Myl2, abnormal modeling of the heart and

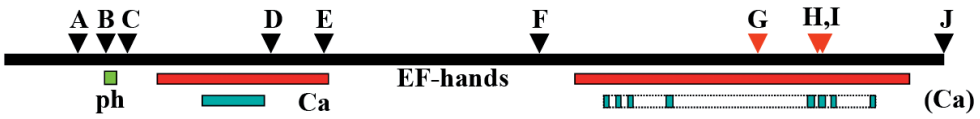

Figure 7: Distribution of dominant *MYL2* mutations in hypertrophic cardiomyopathy and currently described recessive *MYL2* mutations.
(*A-F, J*) The location of dominant missense mutations in patients with hypertrophic cardiomyopathy are indicated by the black triangles (A13T, F18L, E22K, N47K, R58Q, P95A, and D166V) and (*G-I*) the recessive *MYL2* mutations in light chain myopathy patients by the red triangles. The EF-hand domains are indicated by red bars, the green bar indicates the phosphorylation site (ph), the turquoise bar at the left indicates the calcium-binding site (Ca), and at the right site predicted calcium-binding sites are shown (www.ncbi.nih.gov).

abnormal cross-bridge functions were found despite the low percentage of mutant cells and a poison-peptide mechanism was therefore suggested (Kazmierczak *et al.*, 2012), which is in line with the dominant nature of these missense mutations. The other four reported variations, two missense and two splice site mutations, affect the C-terminal part of MYL2, which contains the second EF-hand motif. A functional effect was only shown for the mutation affecting the very last codon (D166V) of MYL2. Myofibril preparations of D166V transgenic mice showed altered cross-bridge kinetics with actin, after induced contraction (Muthu, *et al.*, 2010). Acto-myosin cross-bridges deliver cyclic impulses to actin, resulting in periodic fluctuations of orientation. An irregular pattern of such fluctuations was observed in fibres carrying the mutation compared with the wild type controls, possibly bearing relevance to the origin of myofibrillar disorganization. Myofibrillar disarray, which is a relatively rare phenomenon in pediatric neuromuscular disorders, is a common finding in heart muscle in HCM. Myofibrillar disarray in type I muscle fibres in the present disease carries morphological similarity to the myofibrillar disarray in myocardial muscle cells, and the same mechanism may cause the micro-architectonic disturbance in both cell types.
The splice site mutation we identified here was reported previously in a patient with HCM in a heterozygous state, in combination with another heterozygous variation leading to a K104E change in a family with HCM. The K104E variation was regarded as a likely benign variant, as all four carriers of this change only were asymptomatic with normal electrocardiograms, even late in adulthood (Andersen *et al.*, 2001). In retrospect, the compound heterozygosity may have been responsible for the disease, with one mutant allele only partially complementing the other mutant allele. The parents of the present patients were all heterozygous carriers of the *MYL2* splice site mutation and their ages ranged from 30-69 years at the time of examination, but with cardiological examination only a structural variation of unknown clinical significance was found in one case. To date, no sudden cardiac deaths have been reported in carriers with the splice site mutation (Andersen *et al.*, 2001). Although based on a limited number of families, mutations in this part of the protein may be considered more benign and may only

lead to severe problems in a homozygous state indicative of a loss of function mechanism. A long-term follow-up is needed to establish the potential risk for carriers of a C-terminal truncating mutation of the MYL2 protein.

A complete loss of function has been reported in a severely affected homozygous *Myl2* -/- mouse model (Chen *et al.*, 1998) while heterozygous animals were completely normal (Minamisawa *et al.*, 1999). The mice died at embryonic day 12.5 with dilated cardiomyopathy bearing a resemblance to the human cardioskeletal myopathy reported here. Moreover, ultrastructural defects in sarcomeric assembly of embryonic cardiomyocytes were also present. In the embryonic ventricle of the mutant *Myl* -/- mice, expression of the atrial form of myosin regulatory light chain was found to be significantly higher while in their normal counterparts it was downregulated from this point in development. Analogous to this situation, in the human heart of our patients, MYL2 may have been partially replaced by MYL7, a human cardiac-specific atrial isoform with a weak ventricular expression. However, after birth, the expression of *MYL7* sharply declines (Hailstones *et al.*, 1992), which coincides with the onset of cardiac problems. In muscle, a similar replacement may theoretically also have occurred by other regulatory light chains, which, inadequately have taken over the role of MYL2. Alternatively, if there is residual mutant MYL2 in the myosin complex, it probably affects myosin function. Because neuromuscular and cardiac functioning were apparently normal in all patients at the time of birth, failing adaptation to increased postnatal force requirements may also explain the onset and progression of muscular pareses after birth.

Since the N-terminal EF-hand structure and the consensus calcium-binding site, as well as the phosphorylation site, are still intact in our patients, the exact mechanisms that lead to the disease are currently unknown. Except for the interaction with the myosin heavy chain, MYL2 associations have also been described with three E3 ubiquitin ligases, MURF1/TRIM63/RNF28 (Kedar *et al.*, 2004), MURF2/TRIM55/RNF29 and LRSAM1, a ubiquitously expressed E3 ligase involved in a hereditary motor and sensory neuropathy (Weterman *et al.*, 2012). MURF proteins are thought to be involved in triggering protein degradation during pathophysiological muscle wasting. Ubiquitylation is a process relevant for the balance of hypertrophy and atrophy. A search for MURF1 interactors identified muscle-type creatine kinase, an essential enzyme for energy metabolism (Koyama *et al.*, 2008), and troponin, leading to the suggestion of a role in the balance of hypertrophy and atrophy as well as contractility responses during heart failure. Yeast two-hybrid screens identified more interactions with 11 enzymes required for ATP/energy production in muscle. This clearly shows a link with the coordination of energy metabolism (Witt *et al.*, 2005), which may explain some of the findings that were suggestive of a metabolic defect in the first five patients (Barth *et al.*, 1998). During embryonic development, *Murf2* is specifically expressed at the very onset of cardiac development and small interfering RNA knockdown experiments of *Murf2* in neonatal rat cardiomyocytes disrupts post-translational microtubule modification and myofibril assembly (Perera *et al.*, 2011). Disturbance of interactions of MYL2 with the MURF proteins may well be reflected in

the clinical phenotype we observe in our patients who have no normal MYL2 protein.
In conclusion, identification of several recessive mutations affecting the same exon of *MYL2* with similar effects on the protein has solved the genetic basis of this disorder that presented with clinical findings suggestive of a metabolic disorder rather than a primary cardiomyopathy. Its hallmarks are a rapidly progressive myopathy with hypotrophy of type I fibres, myofibrillar disarray and cardiomyopathy. This study defines this disorder as a new hereditary myosinopathy and extends the clinical range of symptoms due to mutations in myosins. In the case of the currently reported *MYL2* mutations, they cause a very severe phenotype with morphologic and structural skeletal abnormalities in addition to a cardiomyopathy that leads to early infant death.

Acknowledgements
The authors thank B. van Schaik (KEBB, AMC) for her analysis of the exome data, Prof. dr. S. van Duinen (Department of Pathology, LUMC) and Dr. M. van Dijk (Department of Pathology, UMCG) for their assistance with the muscle tissue sections, Prof. dr. O. Milanesi and Dr. E. Opocher (Department of Paediatrics, University of Padua, Italy) for their original contact regarding the Italian family, M. van den Bergh Weerman for his assistance with the EM studies (Department of Pathology, AMC), Dr. A.M.C. Vermeer (Department of Clinical Genetics, AMC) for counseling some of the families, Prof dr S. Clur (Deptartment of Paediatric Cardiology, AMC) for her cardiac expertise, M. Doimo (Department of Paediatrics, University of Padua) for her biochemical and genetic analyses of the Italian samples, and Dr. R. Lekanne (Department of Clinical Genetics, AMC) for critical reading of the manuscript. This research was partially funded by Telethon GUP07OO1 and Eurobiobank.

REFERENCES

1. Abecasis GR, Cherny SS, Cookson WO, Cardon LR. GRR: graphical representation of relationship errors. Bioinformatics 2001; 17: 742-743.
2. Andersen PS, Havndrup O, Bundgaard H, Moolman-Smook JC, Larsen LA, Mogensen J *et al.*, Myosin light chain mutations in familial hypertrophic cardiomyopathy: phenotypic presentation and frequency in Danish and South African populations. J Med Genet 2001a; 38: E43.
3. Barth PG, Wanders RJ, Ruitenbeek W, Roe C, Scholte HR, van der Harten H *et al.*, Infantile fibre type disproportion, myofibrillar lysis and cardiomyopathy: a disorder in three unrelated Dutch families. Neuromuscul Disord 1998; 8: 296-304.
4. Brandis A, Aronica E, Goebel HH. TPM2 mutation. Neuromuscul Disord 2008; 18: 1005.
5. Budde BS, Namavar Y, Barth PG, Poll-The BT, Nurnberg G, Becker C *et al.*, tRNA splicing endonuclease mutations cause pontocerebellar hypoplasia. Nat Genet 2008; 40: 1113-1118.
6. Chen J, Kubalak SW, Minamisawa S, Price RL, Becker KD, Hickey R *et al.*, Selective requirement of myosin light chain 2v in embryonic heart function. J Biol Chem 1998; 273: 1252-1256.
7. Clarke NF, North KN. Congenital fiber type disproportion--30 years on. J Neuropathol Exp Neurol 2003; 62: 977-989.
8. Clarke NF, Kidson W, Quijano-Roy S, Estournet B, Ferreiro A, Guicheney P *et al.*, SEPN1: associated with congenital fiber-type disproportion and insulin resistance. Ann Neurol 2006; 59: 546-552.
9. Clarke NF, Kolski H, Dye DE, Lim E, Smith RL, Patel R *et al.*, Mutations in TPM3 are a common cause of congenital fiber type disproportion. Ann Neurol 2008; 63: 329-337.
10. Clarke NF, Waddell LB, Cooper ST, Perry M, Smith RL, Kornberg AJ *et al.*, Recessive mutations in RYR1 are a common cause of congenital fiber type disproportion. Hum Mutat 2010; 31: E1544-E1550.
11. Darin N, Tajsharghi H, Ostman-Smith I, Gilljam T, Oldfors A. New skeletal myopathy and cardiomyopathy associated with a missense mutation in MYH7. Neurology 2007; 68: 2041-2042.
12. Davis JS, Hassanzadeh S, Winitsky S, Lin H, Satorius C, Vemuri R, Aletras AH, Wen H, Epstein ND. The overall pattern of cardiac contraction depends on a spatial gradient of myosin regulatory light chain phosphorylation. Cell 2001; 107: 631-641.
13. Dubowitz V. Definition of pathological changes seen in muscle biopsies. In: Dubowitz V., ed. Muscle Biopsy. A Practical Approach, 2nd edn. London: Baillière Tindall, 1985; 82-128.
14. Flavigny J, Richard P, Isnard R, Carrier L, Charron P, Bonne G *et al.*, Identification of two novel mutations in the ventricular regulatory myosin light chain gene (MYL2) associated with familial and classical forms of hypertrophic cardiomyopathy. J Mol Med (Berl) 1998; 76: 208-214.
15. Grey C, Mery A, Puceat M. Fine-tuning in Ca2+ homeostasis underlies progression of cardiomyopathy in myocytes derived from genetically modified embryonic stem cells. Hum Mol Genet 2005; 14: 1367-1377.
16. Gudbjartsson DF, Jonasson K, Frigge ML, Kong A. Allegro, a new computer program for multipoint linkage analysis. Nat Genet 2000; 25: 12-13.
17. Hailstones D, Barton P, Chan-Thomas P, Sasse S, Sutherland C, Hardeman E *et al.*, Differential regulation of the atrial isoforms of the myosin light chains during striated muscle development. J Biol Chem 1992; 267: 23295-23300.

18. Hang CT, Yang J, Han P Cheng H-L, Shang C, Euan Ashley *et al.*, Chromatin regulation by Brg1 underlies heart muscle development and disease. Nature 2010; 466: 62-67.

19. Harrison BC, Allen DL, Leinwand LA. IIb or not IIb? Regulation of myosin heavy chain gene expression in mice and men. Skelet Muscle 2011; 1: 5.

20. Kabaeva ZT, Perrot A, Wolter B, Dietz R, Cardim N, Correia JM *et al.*, Systematic analysis of the regulatory and essential myosin light chain genes: genetic variants and mutations in hypertrophic cardiomyopathy. Eur J Hum Genet 2002; 10: 741-748.

21. Kazmierczak K, Muthu P, Huang W, Jones M, Wang Y, Szczesna-Cordary D. Myosin regulatory light chain mutation found in hypertrophic cardiomyopathy patients increases isometric force production in transgenic mice. Biochem J 2012; 442: 95-103.

22. Kedar V, McDonough H, Arya R, Li HH, Rockman HA, Patterson C. Muscle-specific RING finger 1 is a bona fide ubiquitin ligase that degrades cardiac troponin I. Proc Natl Acad Sci U S A 2004; 101: 18135-18140.

23. Kelly DP, Strauss AW. Inherited cardiomyopathies. N Engl J Med 1994; 330: 913-919.

24. Kerrick WG, Kazmierczak K, Xu Y, Wang Y, Szczesna-Cordary D. Malignant familial hypertrophic cardiomyopathy D166V mutation in the ventricular myosin regulatory light chain causes profound effects in skinned and intact papillary muscle fibers from transgenic mice. FASEB J 2009; 23: 855-865.

25. Koyama S, Hata S, Witt CC, Ono Y, Lerche S, Ojima K *et al.*, Muscle RING-finger protein-1 (MuRF1) as a connector of muscle energy metabolism and protein synthesis. J Mol Biol 2008; 376: 1224-1236.

26. Laing NG, Clarke NF, Dye DE, Liyanage K, Walker KR, Kobayashi Y *et al.*, Actin mutations are one cause of congenital fibre type disproportion. Ann Neurol 2004; 56: 689-694.

27. Laing NG, Laing BA, Meredith C, Wilton SD, Robbins P, Honeyman K *et al.*, Autosomal dominant distal myopathy: linkage to chromosome 14. Am J Hum Genet 1995; 56: 422-427.

28. Li Y, Wu G, Tang Q, Jiang H, Shi L, Tu X *et al.*, Slow cardiac myosin regulatory light chain 2 (MYL2) was down-expressed in chronic heart failure patients. Clin Cardiol 2011; 34: 30-34.

29. Lowey S, Waller GS, Trybus KM. Skeletal muscle myosin light chains are essential for physiological speeds of shortening. Nature 1993; 365: 454-456.

30. Macera MJ, Szabo P, Wadgaonkar R, Siddiqui MA, Verma RS. Localization of the gene coding for ventricular myosin regulatory light chain (MYL2) to human chromosome 12q23-q24.3. Genomics 1992; 13: 829-831.

31. Minamisawa S, Gu Y, Ross J, Jr., Chien KR, Chen J. A post-transcriptional compensatory pathway in heterozygous ventricular myosin light chain 2-deficient mice results in lack of gene dosage effect during normal cardiac growth or hypertrophy. J Biol Chem 1999; 274: 10066-10070.

32. Muelas N, Hackman P, Luque H, Garces-Sanchez M, Azorin I, Suominen T *et al.*, MYH7 gene tail mutation causing myopathic profiles beyond Laing distal myopathy. Neurology 2010; 75: 732-741.

33. Muthu P, Mettikolla P, Calander N, Luchowski R, Gryczynski I, Gryczynski Z *et al.*, Single molecule kinetics in the familial hypertrophic cardiomyopathy D166V mutant mouse heart. J Mol Cell Cardiol 2010; 48: 989-998.

34. Nakao K, Minobe W, Roden R, Bristow MR, Leinwand LA. Myosin heavy chain gene expression in human heart failure. J Clin Invest 1997; 100: 2362-2370.

35. Ortolano S, Tarrio R, Blanco-Arias P, Teijeira S, Rodriguez-Trelles F, Garcia-Murias M *et al.*, A novel MYH7 mutation links congenital fiber type disproportion and myosin storage myopathy. Neuromuscul Disord 2011; 21: 254-262.

36. Perera S, Holt MR, Mankoo BS, Gautel M. Developmental regulation of MURF ubiquitin ligases and autophagy proteins nbr1, p62/SQSTM1 and LC3 during cardiac myofibril assembly and turnover. Dev Biol 2011; 351: 46-61.

37. Poetter K, Jiang H, Hassanzadeh S, Master SR, Chang A, Dalakas MC *et al.*, Mutations in either the essential or regulatory light chains of myosin are associated with a rare myopathy in human heart and skeletal muscle. Nat Genet 1996; 13: 63-69.

38. Richard P, Charron P, Carrier L, Ledeuil C, Cheav T, Pichereau C *et al.*, Hypertrophic cardiomyopathy: distribution of disease genes, spectrum of mutations, and implications for a molecular diagnosis strategy. Circulation 2003; 107: 2227-2232.

39. Ruschendorf F, Nurnberg P. ALOHOMORA: a tool for linkage analysis using 10K SNP array data. Bioinformatics 2005; 21: 2123-2125.

40. Rutsch F, Gailus S, Miousse IR, Suormala T, Sagné C, Toliat MR *et al.*, Identification of a putative lysosomal cobalamin exporter altered in the cblF defect of vitamin B12 metabolism. Nat Genet 2009; 41: 234-239.

41. Sanoudou D, Beggs AH. Clinical and genetic heterogeneity in nemaline myopathy--a disease of skeletal muscle thin filaments. Trends Mol Med 2001; 7: 362-368.

42. Schiaffino S, Reggiani C. Fiber types in mammalian skeletal muscles. Physiol Rev 2011; 91: 1447-1531.

43. Szczesna D, Ghosh D, Li Q, Gomes AV, Guzman G, Arana C *et al.*, Familial hypertrophic cardiomyopathy mutations in the regulatory light chains of myosin affect their structure, Ca2+ binding, and phosphorylation. J Biol Chem 2001; 276: 7086-7092.

44. Szczesna-Cordary D, Guzman G, Ng SS, Zhao J. Familial hypertrophic cardiomyopathy-linked alterations in Ca2+ binding of human cardiac myosin regulatory light chain affect cardiac muscle contraction. J Biol Chem 2004; 279: 3535-3542.

45. Szczesna-Cordary D, Guzman G, Zhao J, Hernandez O, Wei J, Diaz-Perez Z. The E22K mutation of myosin RLC that causes familial hypertrophic cardiomyopathy increases calcium sensitivity of force and ATPase in transgenic mice. J Cell Sci 2005; 118: 3675-3683.

46. Tajsharghi H, Thornell LE, Lindberg C, Lindvall B, Henriksson KG, Oldfors A. Myosin storage myopathy associated with a heterozygous missense mutation in MYH7. Ann Neurol 2003; 54: 494-500.

47. Thiele H, Nurnberg P. HaploPainter: a tool for drawing pedigrees with complex haplotypes. Bioinformatics 2005; 21: 1730-1732.

48. Uyeda TQ, Spudich JA. A functional recombinant myosin II lacking a regulatory light chain-binding site. Science 1993; 262: 1867-1870.

49. van Rooij E, Sutherland LB, Qi X, Richardson JA, Hill J, Olson EN. Control of stress-dependent cardiac growth and gene expression by a microRNA. Science 2007; 316: 575-579.

50. VanBuren P, Waller GS, Harris DE, Trybus KM, Warshaw DM, Lowey S. The essential light chain is required for full force production by skeletal muscle myosin. Proc Natl Acad Sci U S A 1994; 91: 12403-12407.

51. Wadgaonkar R, Shafiq S, Rajmanickam C, Siddiqui MA. Interaction of a conserved peptide domain in recombinant human ventricular myosin light chain-2 with myosin heavy chain. Cell Mol Biol Res 1993; 39: 13-26.

52. Walsh R, Rutland C, Thomas R, Loughna S. Cardiomyopathy: a systematic review of disease-causing mutations in myosin heavy chain 7 and their phenotypic manifestations. Cardiology 2010; 115: 49-60.

53. Weiss A, Leinwand LA. The mammalian myosin heavy chain gene family. Annu Rev Cell Dev Biol 1996; 12: 417-439.

54. Weterman MA, Sorrentino V, Kasher PR, Jakobs ME, van Engelen BG, Fluiter K *et al.*, A frameshift mutation in LRSAM1 is responsible for a dominant hereditary polyneuropathy. Hum Mol Genet 2012; 21: 358-370.

55. Wimberly B, Thulin E, Chazin WJ. Characterization of the N-terminal half-saturated state of calbindin D9k: NMR studies of the N56A mutant. Protein Sci 1995; 4: 1045-1055.

56. Witt SH, Granzier H, Witt CC, Labeit S. MURF-1 and MURF-2 target a specific subset of myofibrillar proteins redundantly: towards understanding MURF-dependent muscle ubiquitination. J Mol Biol 2005; 350: 713-722.

SUPPLEMENTARY DATA

Table S1: Sequences of primers used

Gene	Exon	Direction	Sequence 5'-3'
ACACB	1	forward reverse	TTTCTCCTGTCTGACCTTTTCC GGAGGGTGGTAGGGAGTTTC
ACACB	46*	forward reverse	CCGCCAGATTAAAAAGAGCA CAGAGAAACAGGCACTGAGC
FOXN4	1	forward reverse	GGGATGGGTTTGCAGAAGT TGACCTCAGTGACCTGCAC
KCTD10+UBE3B	1	forward reverse	CTCCTCTCGGTCCCTTCTTA ACCTTTATTCGCCGGAGGT
MMAB+MVK	1	forward reverse	ATTGGTTCGCAGTTCTCACC TGAGCCACAGAAGCTGGA
C12orf34	1a	forward reverse	CGCTGTTCTTTGCAACCTG GGAGGTCTCCGTTCAGCAG
C12orf34	1b*	forward reverse	GTAAAACGACGGCCAGTGAGC- GAGAGGAAGCAACAAA AGCCTAGGACCCCTTCTGTC
TRPV4	9	forward reverse	ATTCTCGCCGCTGTTCTTT CCAGGTCTCAGCTACCACGA
GLTP1	1*	forward reverse	TTAGGGGTGTCTAGGGCAGA CACACCTGGGGAAGACTCAC
ANKRD13A	1a	forward reverse	GTGCCCAAGGTCGCCTAT TAGGAGGTGCAGGGGGTAGT
ANKRD13A	1b*	forward reverse	CCCTACGCTCGCTTGCTC GACAGAGGGCTGGAAATGG
IFTD81	1a	forward reverse	GCCCGCTTTGCAAGTAAG TCGACAGTTCATCCCTCCA
IFTD81	1b	forward reverse	AGCACCTCGCAAGTGGAA CCCTCTTCTAGCGCGAAGTC
IFTD81	18	forward reverse	TTCCTATTAAATGTTTT- GCTTTCTTTT TTCTTTCAAAAATCCATCGTGA
ATP2A2	1	forward reverse	GAGGGAGGGTGGGTCAGG CTAGCTGCAGAAGCCACGTC
C12orf24	1	forward reverse	TATGGTGACCCTCGCGATT CTGCACCAAACGCTCCT
PPTC7	1	forward reverse	AGTAAGCGCTCCCTCCATGT ACGCTAGTGGAGCGGAAGAT
TCTN1	6	forward reverse	AGAAGGGGACTGGTGGTAGC TGCTGTAAAAAGCCATGCTG
ARPC3	5	forward reverse	CTGGGGTCCAAGGATAGAAT TGCCAAGAATCGTTTGTGAG
HVCN1	1b	forward reverse	ACTGGGAGCCTCAGAGCAG AGGCCAAGGAATCAGGAGAC
HVCN1	1c	forward reverse	CCTCTTCTCGGAAGGATCG CAGGGACAAGGGGACTAAGA

MYL2	7	forward reverse	CAGTTCTGAGTGGCTGCAAA CACCCTCCGTCTCAGTTCC
MYL2 RT-PCR	7	forward reverse1 reverse2	ATTACGTTCGGGAAATGCTG GGTACTCGGGGGAGAGAGA ACATGGCCTCTGGATGGAT
CUX2	1	forward reverse	AGCCATTGAGAAAAGCCAAA CGGCGAGATCAATTCCTAAT
CUX2	17a	forward reverse	TCAACAGGGATGCTGTGAAC CCCAGTGGTGGTCGAAGTAG
CUX2	17b*	forward reverse	GCCTTGGTGAAGCAGGAG TCCGACATCTTCTCCCAGAG
CUX2	19	forward reverse	AAATGGGTGTTTGGCAACTC ACCCGCTCCGTACCTAGATT
CUX2	22a	forward reverse	CCAAAATGCCATGTATGCAG CTCTCCTGTTGGGGATGAAG
CUX2	22b	forward reverse	ACTCAGGGGAGCTGGACAA TACCCCATCCTGTTGAGGAG
FAM109A	1*	forward reverse	AGTCCCAGCGGGGAAGAT ATCGGGAGGTGGGAAGAAC
FAM109A	3a	forward reverse	CTGTAAAACGGGACCAGCAT CCTTCCAGAGTCCTGAGTGG
FAM109A	3b	forward reverse	GGCCAACGTACCTTGAGAGT TGGGACTTCCGTCTGAATTT
FAM109A	3c	forward reverse	CCAGAGTCACAGACCGTATCC CCACAGTGCCCATTTTTCAT
FAM109A	3d	forward reverse	TTGGGAAAATCAAGGTCAGG GGCTCTCCAGACACTCCTTG
FAM109A	3e	forward reverse	CTTCCTAGGCGGTGAGTCAG ACAGAGGGAGGATCGGTCA
FAM109A	3f	forward reverse	TAACACCTGCACCTGTGTCC AGGTGCTGGATTCTGAGTGG
FAM109A	3g	forward reverse	AGGCCCTGGATTCTCCTTAG GAGTGCTATGGCCAGGAGAT
FAM109A	3h*	forward reverse	ATCTGCTCCCCCAGTCTCTC AGTCCCATCCCTGCCTTCT
FAM109A	3i*	forward reverse	GGTCCAGGCCTGAAGGTG GCGGGAACATGCTCTTCTAC
FAM109A	3j	forward reverse	CTCCATGGCATCCTGACTCT CATCTGTGAAACGGGGATGT
SH3B2	1	forward reverse	CAGCCGAATCTCCGACTC CCTCCTCTTTCCCCACAAA
SH3B2	2a	forward reverse	GGTGTGTAATGGGGCCTACA CCTGTGTCCCGGTAGTCG
SH3B2	2b	forward reverse	GCGAGTTCTGTGAGTTGCAC CTCCAGGGCAGGAACTTCT

Note: All primers were M13-tagged with the exception of the MYL2 RT-PCR primers. PCRs marked with an asterisk were performed with the addition of 5% dimethylsulfoxide in the reaction mixture.

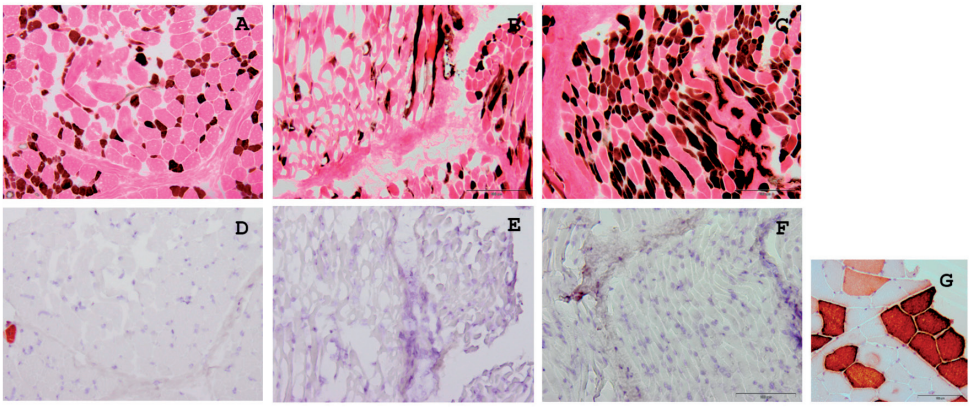

Figure S1: MYL2 expression in frozen muscle sections
Staining for ATPase 4.3 activity on frozen muscle sections of patients N-E1, N-G1 and N-H2 *(A-C)* and immunohistochemical staining of corresponding consecutive sections with antibody 2742-2 *(D-F)*. *G*: Immunohistochemical staining of a frozen control muscle section, simultaneously performed as a positive control.

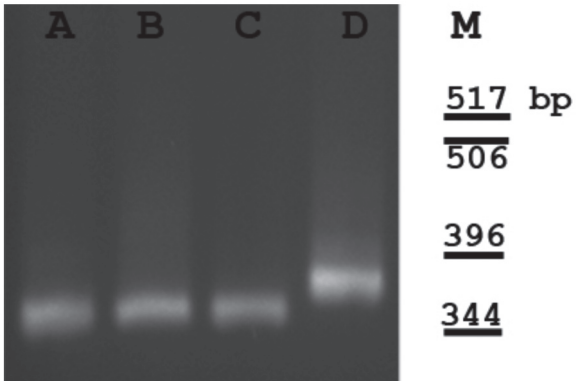

Figure S2: Reverse-transcriptase-PCR analysis of *MYL2* in control and patient tissue
Lane A-C contain the RT-PCR products of normal heart (*A,B*), normal muscle *(C*), or patient N-C2 mRNA *(D)*. For normal tissues, 1 µg of total RNA was used for the PCR reaction, for the N-C2 sample, 5 µg was used. As a reverse primer, the most 3'reverse primer was used.

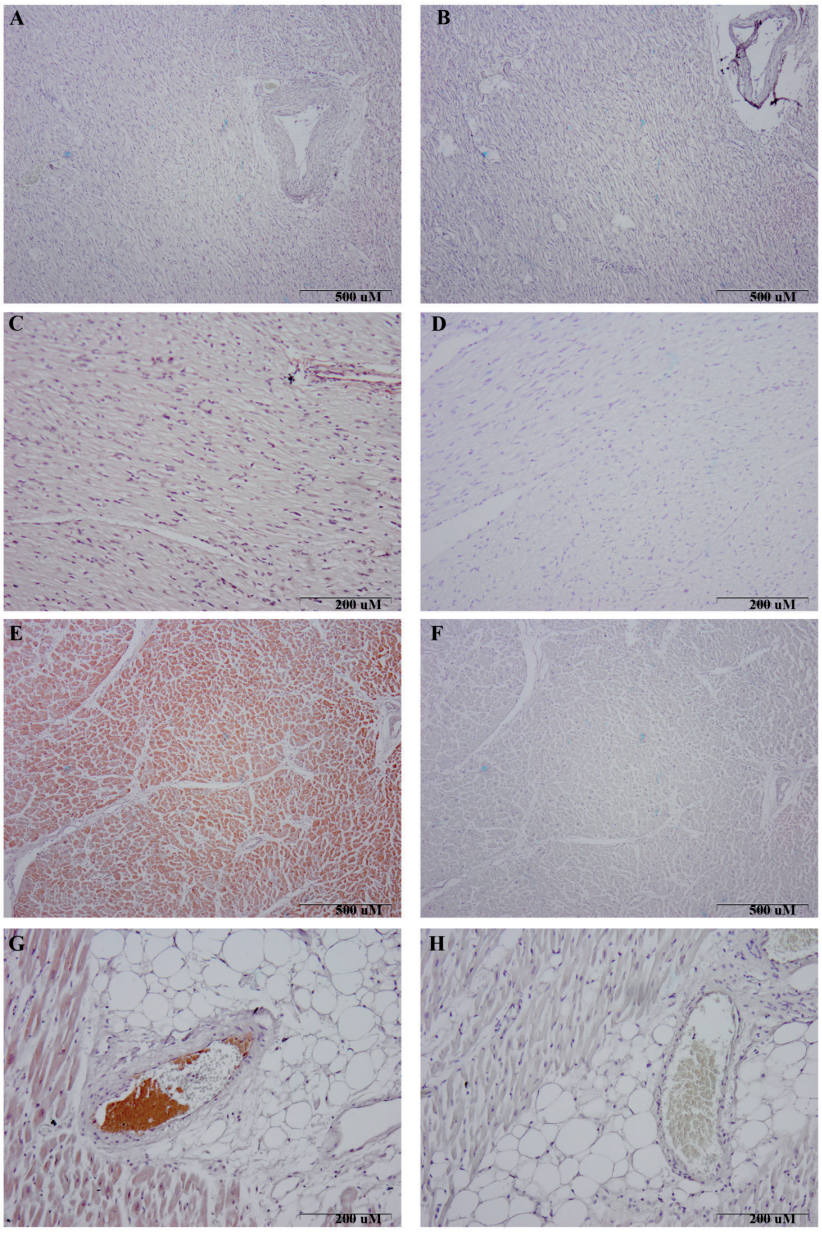

Figure S3: Expression of MYL2 in heart tissue of controls and patients
Panels A, C, E, G show immunoreactivity with antibody 2917-1, panels B, D, F, and H are the corresponding blanks (no primary antibody). The tissues used were from post-mortem heart tissue from patient N-D1 *(A,B)*, patient N-C2 *(C,D)*, and post-mortem heart tissue from two controls *(E,F and G,H)* showing a weak to absent signal for the MYL2 staining while in control material clear expression is present.